Heterogeneous Catalysis

DOI: 10.1002/anie.201007229

Mesoporous Multicomponent Nanocomposite Colloidal Spheres: Ideal High-Temperature Stable Model Catalysts**

*Chen Chen, Caiyun Nan, Dingsheng Wang, Qiao Su, Haohong Duan, Xiangwen Liu, Lesheng Zhang, Deren Chu, Weiguo Song, Qing Peng, and Yadong Li**

Catalysis—the basis of modern chemical industry— plays a vital role in petroleum refining and in applications in medicine, energy, and the environment; therefore, it has high significance for our life. Supported noble-metal catalysts are among the most important catalysts for industrial applications.[1] During the past few decades, extensive research efforts have focused on the effect of particle size of noble metals, the nature of the supporting materials (commonly oxides), and the surface and interfacial effect to improve the performance of these catalysts, and great progress has been achieved.[2–4] However, many intractable problems still exist that hinder the development of this field; one of them is the thermal stability of the catalysts.[5] In supported noble-metal catalysts the metal particles tend to aggregate during the reaction process, and the particle size thus becomes larger which leads to lower catalytic activity. Additionally, the metal particles usually detach from the support when the corresponding catalyst is rubbed reciprocally, which results in a sharp decrease of the active sites. Therefore, the design of an ideal nanostructure for supported noble-metal catalysts that can overcome the above-mentioned limits and, thus, display high stability, is a great challenge in this field.[6]

To address the problems of particle aggregation and detachment from the support, metal particles should be effectively separated from each other and firmly immobilized in the support. By consideration of this point, porous-structured materials might be a good candidate as supporting materials. Up to date, there are two main strategies for the preparation of mesoporous materials;[7,8] one resorts to templating reagents.[7] Soft templates (such as triblock copolymers and surfactants) as well as hard templates (such as porous alumina and porous silica) play a key role in directing the formation of porous structures. The other strategy is based on metal-organic frameworks (MOFs) constructed from molecular building blocks.[8] The size and structure of their three-dimensional (3D) pores can be designed by using various molecular struts. In 2005, our group developed a general liquid–solid solution (LSS) strategy to synthesize a diverse range of nanocrystals, including noble-metal and oxide particles.[9,10] And recently, we developed a general emulsion-based bottom-up self-assembly (EBS) strategy to assemble monodisperse nanoparticles (NPs) into 3D colloidal spheres.[11,12]

Herein, we describe a novel structure for preparing thermally stable nanocomposite catalysts: mesoporous multicomponent nanocomposite colloidal spheres (MMNCSs). We use both oxide (CeO_2 and TiO_2) and noble-metal (Ru, Rh, Pd, Pt, Au and Ag) nanoparticles as building block to fabricate the target colloidal spheres (Figure 1). The MMNCSs are expected to be a new type of ideal model catalysts that are stable at high reaction temperatures. As shown in Figure 1, the active sites of a noble metal in traditional supported catalysts decrease rapidly during heating, because NPs tend to aggregate at high temperatures. The displacement of noble-metal NPs on or from the support weakens the synergistic interaction between the noble metal and oxide nanparticles, which accordingly decreases the catalytic activity. In comparison, noble-metal NPs in MMNCSs are encaged within a mesoporous structured shell composed of oxide NPs, which effectively prevent their aggregation and displacement. On the other hand, the reacting molecules can easily access the noble metal through the mesopores within MMNCSs, through which the product molecules can also readily exit. Further-

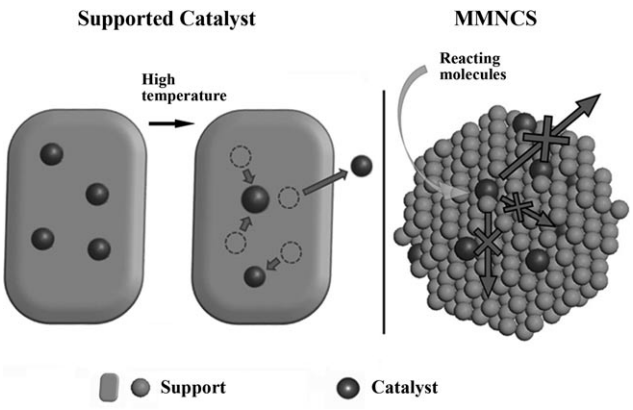

Figure 1. Schematic representation of the MMNCSs as high-temperature model catalysts compared with traditional supported catalysts.

[*] C. Chen, C. Nan, Dr. D. Wang, Q. Su, H. Duan, X. Liu, D. Chu, Dr. Q. Peng, Prof. Y. Li
Department of Chemistry, Tsinghua University
Beijing, 100084 (P.R. China)
Fax: (+86) 10-6278-8765
E-mail: ydli@mail.tsinghua.edu.cn
L. Zhang, Prof. W. Song
Beijing National Laboratory for Molecular Sciences
Institute of Chemistry, Chinese Academy of Sciences
Beijing, 100190 (P.R. China)

[**] This work was supported by the NSFC (20921001, 90606006) and by the State Key Project of Fundamental Research for Nanoscience and Nanotechnology (2006CB932300).

Supporting information for this article is available on the WWW under http://dx.doi.org/10.1002/anie.201007229.

more, the catalytic activity of MMNCSs for certain reactions (CO oxidation, e.g.) may be enhanced when the particle size of the oxide support decreases down to the nanosize region,[3] which is another advantage of MMNCSs.

The MMNCSs were prepared in four steps: 1) synthesis of noble-metal NPs and oxide NPs,[9] 2) mixing of two or more sorts of NPs in a solvent at a certain ratio, 3) assembly of the mixed NPs into the form of colloidal spheres in accordance with the EBS protocol,[11,12] and 4) calcination of these spheres to obtain mesoporous structures. Transmission electron microscopy (TEM) images of the as-prepared MMNCSs are presented in Figure 2. The images of Ag–CeO_2 MMNCSs (Figure 2a) show that the diameters of the colloidal spheres range from 80 to 100 nm. The ordered mesoporous structures of Ag–CeO_2 MMNCSs are constituted by CeO_2 NPs (ca. 3 nm in diameter) and Ag NPs (ca. 10 nm in diameter). As almost all of the NPs are incorporated in the colloidal spheres, outside which barely any isolated particles are observed, we can infer that there is no mass loss during the assembly process and that the ratio of the two sorts of NPs (Ag and CeO_2) in MMNCSs is consistent with that one used initially. In addition, inductively coupled plasma mass spectrometry (ICP-MS) analysis also confirmed the total conversion (5.39 wt% Ag before the assembly and 5.34 wt% after the assembly). Therefore, the mass fraction of Ag NPs in Ag–CeO_2 MMNCSs is speculated to be approximately 5%. The sort and ratio of NPs in MMNCSs can be tuned in the assembly process. Figure 2b shows ternary (Ag–TiO_2–CeO_2) MMNCSs, and the mass fraction is 5% for the Ag NPs, 45% for the TiO_2 NPs, and 50% for the CeO_2 NPs. Both Figure 2c and 2d show Au–CeO_2 MMNCSs (2 wt% Au), but the diameter of the Au NPs is 5 nm (Figure 2c) and 3 nm (Figure 2d). In Figure 2d it is difficult to distinguish Au NPs from CeO_2 NPs because they are of similar size.

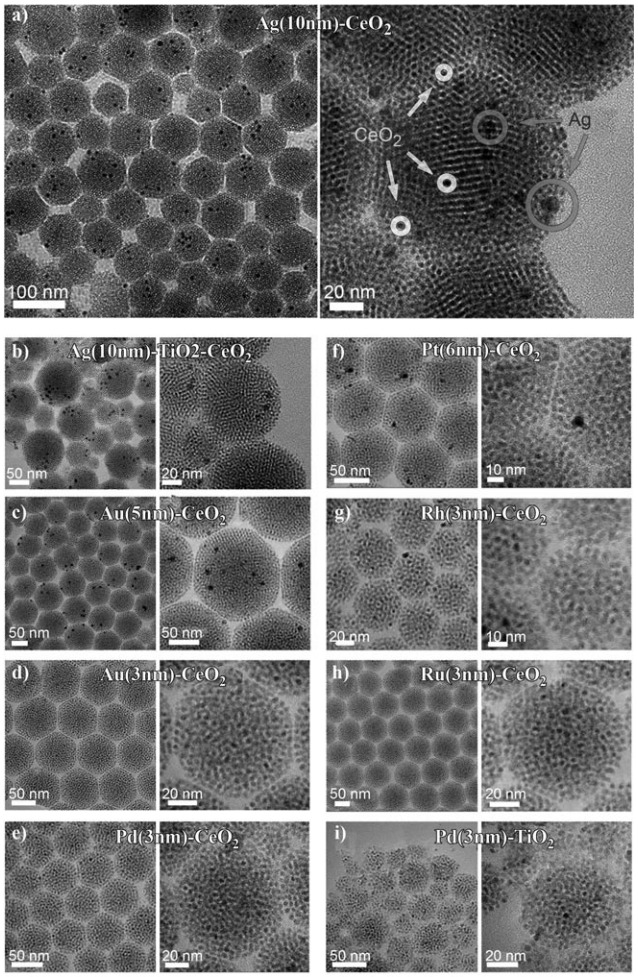

Figure 2. A series of typical TEM images of mesoporous multicomponent nanocomposite colloidal spheres (MMNCS): a) Ag(10 nm)–CeO_2, b) Ag(10 nm)–TiO_2–CeO_2, c) Au(5 nm)–CeO_2, d) Au(3 nm)–CeO_2, e) Pd(3 nm)–CeO_2, f) Pt(6 nm)–CeO_2, g) Rh(3 nm)–CeO_2, h) Ru-(3 nm)–CeO_2, and i) Pd(3 nm)–TiO_2.

It should be noted that the general strategy for preparing MMNCSs is independent of the chemical compositions of the internal building blocks. As a result, we can readily obtain various sorts of MMNCSs, since the preparation techniques of almost all kinds of building blocks of noble metals and oxides are well-established. Figure 2e–i shows a series of MMNCSs assembled from different representative noble-metal and oxide NPs through this strategy, such as Pd–CeO_2 (5 wt% Pd), Pt–CeO_2 (2 wt% Pt), Rh–CeO_2 (2 wt% Rh), Ru–CeO_2 (3 wt% Ru), and Pd–TiO_2 (3 wt% Pd).

To further verify the mesoporous structure of the MMNCSs, we recorded of N_2 adsorption–desorption isotherms and small-angle X-ray diffraction (SAXRD) patterns (Figure 3). The Barrett–Joyner–Halenda (BJH) pore-size distribution curves obtained by analysis of the desorption curve indicate that Au–CeO_2 and Pd–TiO_2 MMNCSs (Figure 3a,b, insets) possess pores with sizes around 1.8 and 2.2 nm, respectively, (corresponding to pores inside the spheres), and their respective Brunauer–Emmett–Teller (BET) surface areas are 92.5 and 242.6 $m^2 g^{-1}$. In addition, a weak peak at a larger pore size is found for each sample, which corresponds to the mesopores among the spheres (see Figure S2 for in the Supporting Information). SAXRD patterns of Au–CeO_2 and Pd–TiO_2 MMNCSs (Figure 3c,d) show primary peaks centered at 4.2 and 4.5 nm, respectively, which indicate that the mesoporous structures are well-ordered. The corresponding TEM images demonstrate that the diameters of the building blocks (mainly the oxide NPs) in Au–CeO_2 and Pd–TiO_2 MMNCSs are approximately 3 and 6–8 nm, respectively. As the TEM results are in good agreement with those deduced from BJH curves, SAXRD patterns, and calculation results,[12] we can qualitatively deduce that the pore size would increase with increasing diameter of the building blocks, which affords a manner to tune the pore size of the mesoporous structures of the MMNCSs.

To investigate the catalytic properties of the MMNCSs as some kind of model catalysts, the activity for CO oxidation was examined for Au–CeO_2 MMNCSs (the corresponding TEM images are shown in Figure 2d). For comparison, the sample of Au NPs supported on bulk CeO_2 with the same particle size (3 nm) and amount (2 wt%) was also tested under the same conditions (see Figure S5 in the Supporting Information). As shown in Figure 4a, Au NPs supported on bulk CeO_2 react with CO at 97.4% conversion when the reaction is performed at 78°C, while Au–CeO_2 MMNCSs

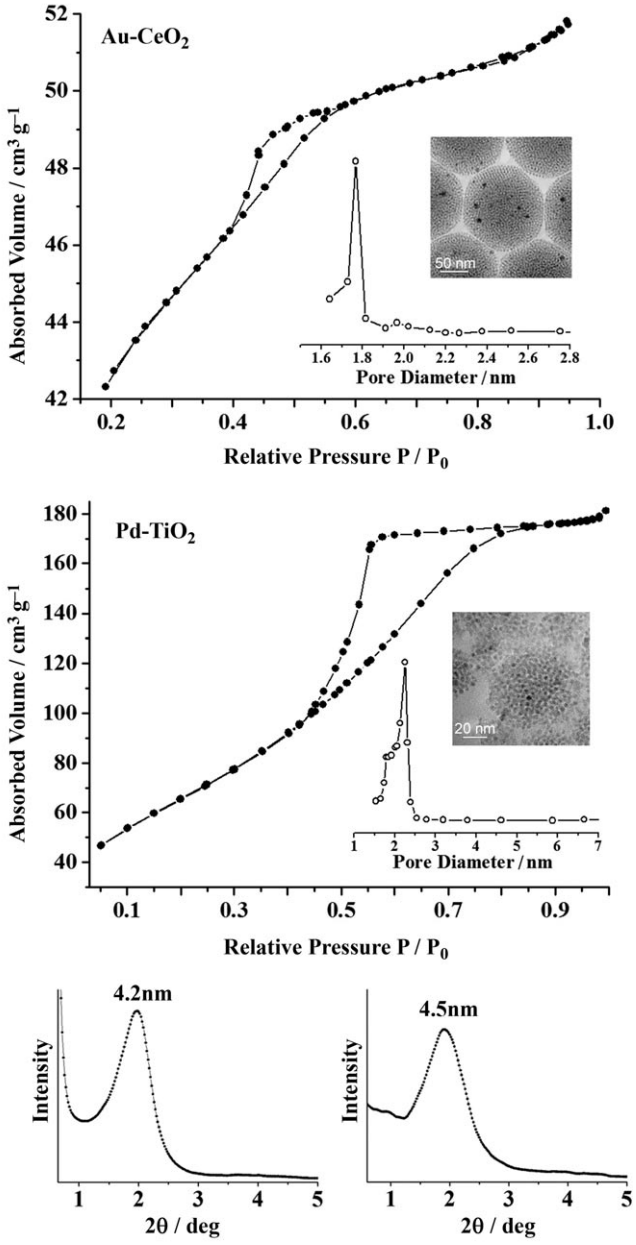

Figure 3. N_2 adsorption–desorption isotherms, pore size distribution curves, and the corresponding TEM images (inset) for two typical MMNCSs: a) Au–CeO_2, b) Pd–TiO_2; small-angle X-ray diffraction patterns of the MMNCSs: c) Au–CeO_2, d) Pd–TiO_2.

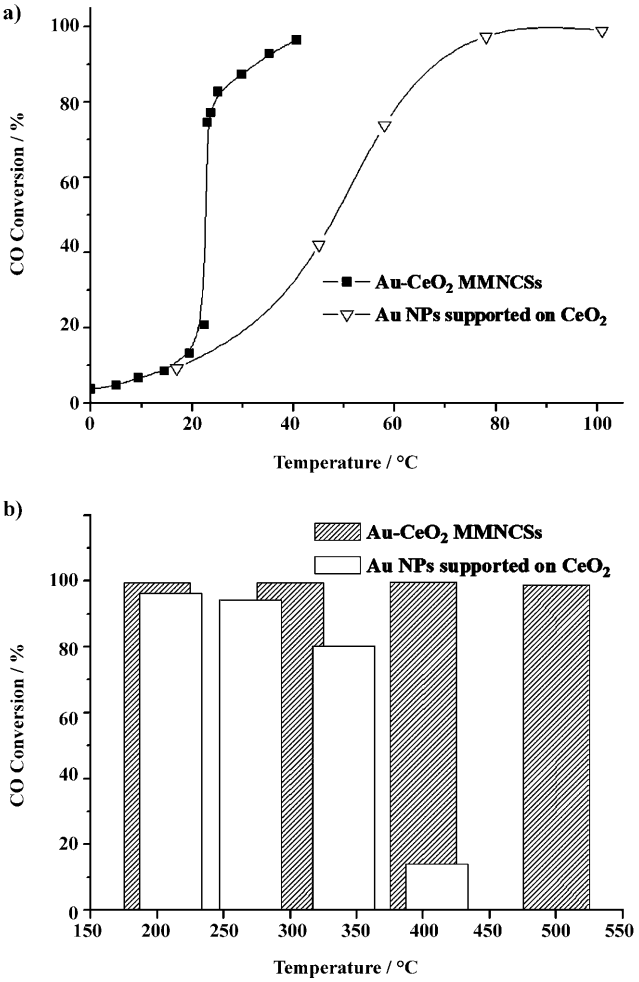

Figure 4. a) Catalytic activity of the Au–CeO_2 MMNCSs and the Au NPs supported on bulk CeO_2 with the same particle size (3 nm) and amount (2 wt%) for CO oxidation. b) CO conversion at 100 °C after the catalytic process had been run continuously for 1 h at different high temperatures.

react with 97.7% conversion at 40 °C. The higher activity of Au–CeO_2 MMNCSs can be attributed to the stronger synergistic interaction between the Au and CeO_2 nanoparticles and to the size effect of CeO_2.

Besides the catalytic activity, the thermal stability of both samples was also examined at high reaction temperature. Figure 4b shows the histogram for CO conversion of Au–CeO_2 MMNCSs and supported Au NPs at 100 °C after the catalytic process had been run continuously for 1 h at different high temperatures. The conversion activity of supported Au NPs decreases slowly after continuous reaction at a temperature below 300 °C. With increasing reaction temperature, the conversion rate decreases rapidly to 80.2% at 100 °C after continuous reaction at about 350 °C and to 14% after continuous reaction at about 415 °C. The sharp decrease in catalytic activity is probably a consequence of particle aggregation and growth of the Au NPs, since it is well-known that Au NPs exhibit considerable catalytic activity only when their sizes are below 10 nm. In strong contrast, the catalytic activity of Au–CeO_2 MMNCSs shows negligible decrease at temperatures up to 500 °C. TEM characterization confirmed that the morphology is not essentially changed after the high-temperature reaction, and the ordered mesoporous structure is basically preserved (see Figure S3 in the Supporting Information). These results indicate that the Au NPs are prevented from aggregation even at a high reaction temperature, which proves the effectiveness of the unique mesoporous structures in MMNCSs. Similar results were also obtained for Au–TiO_2 MMNCS sample (see Figure S4 in the Supporting Information).

We also examined cyclohexene hydroconversion to further study the catalytic properties of MMNCSs, because the

dehydrogenation of cycloalkanes and cycloalkenes into aromatic molecules is one of the key reactions during naphtha reforming. In addition, it was reported that noble-metal NPs of different sizes exhibit different catalytic selectivities for different products; specifically, small particles are more active for dehydrogenation (yielding benzene) than for hydrogenation (yielding cyclohexane).[13] As a result, we employed the cyclohexene hydroconversion as a probe reaction to monitor any possible change in the particle size of the Pd metal. We selected Pd–CeO_2 MMNCSs (corresponding TEM images are shown in Figure 2e) to examine the catalytic activity. CO chemisorption measurements revealed that Pd was dispersed by 34.8% in this sample. As shown in Figure 5, 99.9% of the cyclohexene reacted with hydrogen to give cyclohexane at an

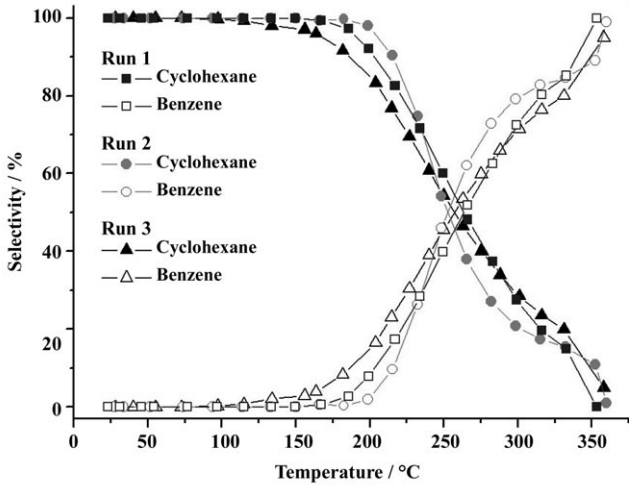

Figure 5. Selectivity of the cyclohexene hydrogenation to cyclohexane (filled symbols) and the dehydrogenation to benzene (empty symbols) with Pd–CeO_2 MMNCSs as catalysts.

ambient temperature. Then, the amount of cyclohexane in the product decreased from 97.2% (at 185°C) to 0% (at 350°C), while the amount of benzene increased from 0.6% (at 167°C) to 99.9% (at 350°C). These results show that Pd–CeO_2 MMNCSs exhibit good selectivity for cyclohexene hydroconversion. Further, the series of experiments were performed for two more cycles, and no significant loss in catalytic activity was observed, which indicates that the MMNCSs display good thermal stability and robust performance.

In summary, the mesoporous multicomponent nanocomposite colloidal spheres, assembled from noble-metal and oxide NPs, were designed as a new type of high-temperature model catalysts. The unique structure endows the MMNCSs with high catalytic activity and thermal stability at high temperatures for both CO oxidation and cyclohexene hydroconversion. The strategy is independent of the chemical composition of the building blocks, and hence can be extended to other composite catalysts, such as three-way catalysts. The close contact of multicomponent NPs in the MMNCSs also provides the possibility of further research in the synergistic interaction between noble-metal and oxide nanoparticles. These catalysts can potentially be used in many important high-temperature reactions in industry, such as partial oxidation and cracking of hydrocarbons as well as catalytic combustion.

Experimental Section

Synthesis of CeO_2 nanoparticles: NaOH (0.5 g) was dissolved in deionized water (10 mL), and then ethanol (15 mL) and oleic acid (4 mL) were added to form a clear solution under stirring. $(NH_4)_2Ce(NO_3)_6$ (2 g) was dissolved in water (10 mL) and added dropwise to the mixed solvent to form a yellow precipitate. The reactant mixture was then transferred into a 40 mL Teflon-lined autoclave and heated at 180°C for 10 h. After the autoclave had been allowed to cool to room temperatur, the CeO_2 NPs were directly collected at the bottom of the vessel.

Synthesis of Au nanoparticles: An orange precursor solution of tetralin (10 mL), oleylamine (10 mL), and $HAuCl_4{\cdot}3H_2O$ (0.1 g) was prepared in air at 25°C and it was stirred under N_2 flow for 10 min. Then, a reducing solution containing *tert*-Butylamine borane (0.5 mmol), tetralin (1 mL), and oleylamine (1 mL) was mixed by sonication and injected into the precursor solution. The mixture was allowed to react at 25°C for 1 h before acetone was added to precipitate the Au NPs. The Au NPs were collected by centrifugation and redispersed in hexane.

Assembly of mesoporous multicomponent nanocomposite colloidal spheres: CeO_2 NPs (9.8 mg) and Au NPs (0.2 mg) were mixed in cyclohexane (1 mL), and then added to of an aqueous solution of sodium dodecylsulfate (SDS; 3 mg mL^{-1}; 10 mL). This mixture was then emulsified by ultrasonic treatment. Cyclohexane was removed by heating at 70°C with constant stirring for 2 h to assemble the NPs into MMNCSs. The products were collected and purified by repeated centrifugation, and then redispersed in deionized water.

Calcination of colloidal spheres: The calcination treatments were carried out in air at 200°C for 2 h.

Similar synthetic procedures were used for other MMNCSs (see the Supporting Information).

Received: November 17, 2010
Published online: March 21, 2011

Keywords: heterogeneous catalysis · mesoporous materials · nanocomposites · nanoparticles · thermal stability

[1] a) A. Grirrane, A. Corma, H. Garcia, *Science* **2008**, *322*, 1661–1664; b) M. Boronat, P. Concepcion, A. Corma, S. Gonzalez, F. lllas, P. Serna, *J. Am. Chem. Soc.* **2007**, *129*, 16230–16237; c) M. Haruta, N. Yamada, T. Kobayashi, S. J. Iijima, *Catalysis* **1989**, *115*, 301–309; d) G. A. Somorjai, Y. G. Borodko, *Catal. Lett.* **2001**, *76*, 1–5.

[2] a) N. F. Zheng, G. D. Stucky, *J. Am. Chem. Soc.* **2006**, *128*, 14278–14280; b) A. Corma, *Chem. Rev.* **1997**, *97*, 2373–2420; c) J. Chane-Ching, F. Cobo, D. Aubert, H. G. Harvey, M. Airiau, A. Corma, *Chem. Eur. J.* **2005**, *11*, 979–987.

[3] a) S. Carrettin, P. Concepcion, A. Corma, J. M. L. Nieto, V. F. Puntes, *Angew. Chem.* **2004**, *116*, 2592–2594; b) V. B. Fainerman, M. E. Leser, M. Michel, E. H. Lucassen-Reynders, R. Miller, *J. Phys. Chem. B* **2005**, *109*, 9672–9677.

[4] J. F. Liu, W. Chen, X. W. Liu, K. B. Zhou, Y. D. Li, *Nano Res.* **2008**, *1*, 46–55.

[5] a) C. T. Campbell, S. C. Parker, D. E. Starr, *Science* **2002**, *298*, 811–814; b) S. H. Joo, J. Y. Park, C. K. Tsung, Y. Yamada, P. D. Yang, G. A. Somorjai, *Nat. Mater.* **2009**, *8*, 126–131; c) L. S. Ott, R. G. Finke, *Coord. Chem. Rev.* **2007**, *251*, 1075–1100.

[6] a) R. Narayanan, M. A. El-Sayed, *J. Am. Chem. Soc.* **2003**, *125*, 8340–8347; b) C. T. Campbell, G. Ertl, H. Kuipers, J. Segner,

J. Chem. Phys. **1980**, *73*, 5862 – 5873; c) X. Su, P. S. Cremer, Y. R. Shen, G. A. Somorjai, *J. Am. Chem. Soc.* **1997**, *119*, 3994 – 4000; d) K. R. McCrea, J. S. Parker, G. A. Somorjai, *J. Phys. Chem. B* **2002**, *106*, 10854 – 10863.

[7] a) S. Costacurta, L. Biasetto, E. Pippel, J. Woltersdorf, P. Colombo, *J. Am. Ceram. Soc.* **2007**, *90*, 2172 – 2177; b) D. Kuang, T. Brezesinski, B. Smarsly, *J. Am. Chem. Soc.* **2004**, *126*, 10534 – 10535; c) T. Sen, G. J. T. Tiddy, J. L. Casci, M. W. Anderson, *Angew. Chem.* **2003**, *115*, 4797 – 4801; *Angew. Chem. Int. Ed.* **2003**, *42*, 4649 – 4653; d) A. Cao, G. Veser, *Nat. Mater.* **2010**, *9*, 75 – 81.

[8] a) V. A. Russell, C. C. Evans, W. J. Li, M. D. Ward, *Science* **1997**, *276*, 575 – 579; b) H. Li, M. Eddaoudi, M. O'Keeffe, O. M. Yaghi, *Nature* **1999**, *402*, 276 – 279; c) H. M. El-Kaderi, J. R. Hunt, J. L. Mendoza-Cortes, A. P. Cote, R. E. Taylor, M. O'Keeffe, O. M. Yaghi, *Science* **2007**, *316*, 268 – 272.

[9] a) X. Wang, J. Zhuang, Q. Peng, Y. D. Li, *Nature* **2005**, *437*, 121 – 124; b) Z. Y. Huo, C. Chen, Y. D. Li, *Chem. Commun.* **2008**, 3741 – 3743; c) S. Peng, Y. Lee, C. Wang, H. F. Yin, S. Dai, S. H. Sun, *Nano Res.* **2008**, *1*, 229 – 234; d) X. L. Li, Q. Peng, Y. D. Li, *Chem. Eur. J.* **2006**, *12*, 2382 – 2391; e) S. W. Kim, J. Park, Y. Jang, Y. Chung, S. Hwang, T. Hyeon, Y. W. Kim, *Nano Lett.* **2003**, *3*, 1289 – 1291.

[10] a) D. S. Wang, T. Xie, Q. Peng, S. Y. Zhang, J. Chen, Y. D. Li, *Chem. Eur. J.* **2008**, *14*, 2507 – 2513; b) D. S. Wang, T. Xie, Y. D. Li, *Nano Res.* **2009**, *2*, 30 – 46.

[11] F. Bai, D. S. Wang, Z. Y. Huo, W. Chen, L. P. Liu, X. Liang, C. Chen, X. Wang, Q. Peng, Y. D. Li, *Angew. Chem.* **2007**, *119*, 6770 – 6773; *Angew. Chem. Int. Ed.* **2007**, *46*, 6650 – 6653.

[12] D. S. Wang, T. Xie, Q. Peng, Y. D. Li, *J. Am. Chem. Soc.* **2008**, *130*, 4016 – 4022.

[13] R. M. Rioux, B. B. Hsu, G. A. Somorjai, *Catal. Lett.* **2008**, *126*, 10 – 19.

